DHHC7-mediated palmitoylation of the accessory protein barttin critically regulates the functions of ClC-K chloride channels

Received for publication, September 11, 2019, and in revised form, March 13, 2020 Published, Papers in Press, March 17, 2020, DOI 10.1074/jbc.RA119.011049

Nataliya Gorinski[‡], Daniel Wojciechowski[§], Daria Guseva[‡], Dalia Abdel Galil[‡], Franziska E. Mueller[‡], Alexander Wirth[‡], Stefan Thiemann[§], Andre Zeug[‡], Silke Schmidt[‡], Monika Zareba-Kozioł[¶1], Jakub Wlodarczyk[¶1], Boris V. Skryabin[‖], Silke Glage[**], Martin Fischer[§], Samer Al-Samir[‡‡], Nicole Kerkenberg[§§¶¶], Christa Hohoff[§§], Weiqi Zhang[§§¶¶], Volker Endeward[‡‡], and Evgeni Ponimaskin[‡2]

From the [‡]Department of Cellular Neurophysiology, [§]Institute for Neurophysiology, [**]Institute for Laboratory Animal Science, and [‡‡]Institute of Vegetative Physiology, Hannover Medical School, 30625 Hannover, Germany, the [¶]Laboratory of Cell Biophysics, Nencki Institute of Experimental Biology, Polish Academy of Sciences, 02-093 Warsaw, Poland, and the [‖]Department of Medicine, Core Facility Transgenic Animal and Genetic Engineering Models (TRAM), the [§§]Department of Psychiatry and Psychotherapy, Laboratory for Molecular Psychiatry, and the [¶¶]Otto Creutzfeldt Center for Cognitive and Behavioral Neuroscience, University of Münster, 48149 Münster, Germany

Edited by Mike Shipston

Barttin is the accessory subunit of the human ClC-K chloride channels, which are expressed in both the kidney and inner ear. Barttin promotes trafficking of the complex it forms with ClC-K to the plasma membrane and is involved in activating this channel. Barttin undergoes post-translational palmitoylation that is essential for its functions, but the enzyme(s) catalyzing this post-translational modification is unknown. Here, we identified zinc finger DHHC-type containing 7 (DHHC7) protein as an important barttin palmitoyl acyltransferase, whose depletion affected barttin palmitoylation and ClC-K-barttin channel activation. We investigated the functional role of barttin palmitoylation *in vivo* in *Zdhhc7*$^{-/-}$ mice. Although palmitoylation of barttin in kidneys of *Zdhhc7*$^{-/-}$ animals was significantly decreased, it did not pathologically alter kidney structure and functions under physiological conditions. However, when *Zdhhc7*$^{-/-}$ mice were fed a low-salt diet, they developed hyponatremia and mild metabolic alkalosis, symptoms characteristic of human Bartter syndrome (BS) type IV. Of note, we also observed decreased palmitoylation of the disease-causing R8L barttin variant associated with human BS type IV. Our results indicate that dysregulated DHHC7-mediated barttin palmitoylation appears to play an important role in chloride channel dysfunction in certain BS variants, suggesting that targeting DHHC7 activity may offer a potential therapeutic strategy for reducing hypertension.

Bartter syndrome (BS)[3] is a group of hereditary autosomal recessive disorders characterized by impaired ion transport across renal epithelia in the ascending limb of Henle's loop. This leads to renal salt-losing nephropathies associated with hypokalemic metabolic alkalosis. BS can generally be divided into five subfamilies. Type I is associated with mutations in the NKCC2 (Na-K-Cl cotransporter) transporter, Type II, with mutations in the potassium ROMK (renal outer medullary potassium) channel, and Type III with mutations in the chloride ClC-Kb channel. BS Type V is characterized by mutations within the calcium-sensing receptor (1), whereas mutations within the barttin protein lead to BS Type IV, a human syndrome that combines sensorineural deafness and a deficit in urinary concentration (2, 3).

Barttin is the accessory subunit of the human ClC-Ka and ClC-Kb chloride channels expressed in both the kidney and the inner ear. Barttin promotes trafficking of the ClC-K/barttin complex to the plasma membrane, increases channel stability, and switches ClC-K/barttin channels into an active state (4, 5). Chloride permeability in the thin and thick ascending loops of Henle is a crucial component in establishing the cortico-medullary osmotic gradient that is a central component of urine concentration (6, 7). Thus, functional regulation of ClC-K channels via barttin is critically involved in adjusting water excretion and intake.

We recently showed that barttin is palmitoylated both *in vivo* and *in vitro* and identified cysteine residues Cys-54 and Cys-56 as the palmitoylation sites (8). Expression of palmitoylation-deficient barttin mutants reduced the macroscopic current

This work was supported by Deutsche Forschungsgemeinschaft (DFG) Grants Po732 (to E. P.) and ZH 34/3-1 (to A. Z.) as well as by the Otto Creutzfeldt Center for Cognitive and Behavioral Neuroscience of the University of Münster and the Interdisciplinary Centre for Clinical Research (IZKF) of the University of Münster Medical School (Zha3-005-14 and core unit PIX). The authors declare that they have no conflicts of interest with the contents of this article.

This article contains Tables S1 and S2 and Figs. S1–S5.

[1] Supported by National Science Centre Grant UMO-2017/26/E/NZ4/00637.

[2] To whom correspondence should be addressed: Institute of Cellular Neurophysiology, Hannover Medical School, Carl-Neuberg-Str. 1, 30625 Hannover, Germany. Tel.: 49-511-532-4855; Fax: 49-511-532-8302; E-mail: Ponimaskin.Evgeni@mh-hannover.de.

[3] The abbreviations used are: BS, Bartter syndrome; ABE, acyl-biotinyl exchange; APEGS, acyl-PEGyl-exchange gel shift; CFP, cyan fluorescent protein; DCT, distal convolute tubule; HA, hemagglutinin; HEK, human embryonic kidney; MDCK, Madin–Darby canine kidney; PAT, palmitoyl acyltransferase; mTAL, medullar thick ascending limb; mTL, medullar thin ascending limb; YFP, yellow fluorescent protein; shRNA, short hairpin RNA; P, postnatal day; qPCR, quantitative PCR; HRP, horseradish peroxidase; GAPDH, glyceraldehyde-3-phosphate dehydrogenase; ANOVA, analysis of variance; eGFP, enhanced green fluorescent protein; KO, knockout.

amplitudes of ClC-K/barttin channels without affecting ClC-K/barttin expression and plasma membrane insertion, demonstrating that barttin palmitoylation is necessary for the activation of plasma membrane-inserted ClC-K/barttin channels (8).

Palmitoylation is the post-translational attachment of palmitate to cysteine residue(s) within the protein via a labile thioester linkage. As palmitoylation can be dynamically regulated, it is now widely accepted that repeated cycles of palmitoylation and depalmitoylation could have important consequences for protein functions (9, 10). Palmitoylation is catalyzed by a family of enzymes containing a DHHC (Asp-His-His-Cys) cysteine-rich domain, which is directly involved in the palmitoyl transfer reaction. A multitude of DHHC proteins exists in eukaryotic cells, including eight in yeast (11, 12) and 23 in humans (13). Various studies, including our own, indicate that DHHC proteins possess distinct but overlapping substrate specificities (14–16). As palmitoylation controls a variety of important cellular processes, it is not surprising that several DHHC proteins are implicated in human disease (17–21). The importance of palmitoylation has also been demonstrated for multiple renal proteins, including ARL13b (ADP-ribosylation factor-like GTPase 13b) (22), DHHC2-mediated palmitoylation of the γ-subunit of epithelial sodium channels (23), and NaPi-II (type II Na/phosphate co-transporter) (24).

In the present study, we identified DHHC7 as the cognate palmitoylating enzyme for barttin and demonstrated the importance of DHHC7-mediated barttin palmitoylation for the activation of ClC-K channels. To investigate the functional role of barttin palmitoylation *in vivo*, we established the *Zdhhc7*$^{-/-}$ mouse line. Palmitoylation of barttin in the kidneys of *Zdhhc7*$^{-/-}$ mice was significantly reduced during development. Moreover, when fed a low-salt diet, DHHC7-deficient mice developed hyponatremia and metabolic alkalosis, symptoms characteristic of the mild form of BS.

Results

DHHC7 is a palmitoyl acyltransferase for barttin

To identify the enzyme(s) palmitoylating barttin, we co-expressed barttin-CFP with each of the 23 HA-tagged mouse DHHC palmitoyl acyltransferases (PATs) in HEK293T cells, followed by metabolic labeling with [9,10-^{3}H(N)]palmitic acid. Substantially increased barttin palmitoylation was observed after co-expression of DHHC3, DHHC6, DHHC7, and DHHC20, whereas barttin expression was comparable with the amount of barttin in cells with endogenously expressed DHHCs (Fig. S1). The role of these DHHCs was further evaluated by the ABE approach, with DHHC3 and DHHC7 as the only PATs, increasing barttin palmitoylation significantly (Fig. 1*A*). Notably, both candidate DHHCs belong to the same subfamily of DHHC proteins, with relatively high sequence homology. The sequence homology between human DHHC3 and DHHC7 is 52%, and even higher between mouse and rat (25). Moreover, each of these DHHCs is highly conserved between different mammalian species, with ~80% homology between mouse, rat, and human isoforms. These two candidate DHHCs are distributed within Golgi compartments. It is notable that DHHC7 is expressed in all parts of the Golgi apparatus (*i.e. trans-*, *medial-*, and *cis*-Golgi), whereas DHHC3 is expressed only in the *cis*-Golgi compartment (26). More importantly, the relative expression of the DHHC7 in kidney is higher than that for the DHHC3 (12).

To evaluate the role of DHHC7 in barttin palmitoylation, we generated a specific short hairpin RNA (shRNA) directed against a noncoding region of *DHHC7* mRNA (Fig. S2*A*). Expression of this shRNA in HEK293T cells significantly reduced the amount of *DHHC7* transcript compared with cells transfected with scrambled shRNA (Fig. 1*B*). Knockdown of endogenous DHHC7 by the shRNA significantly decreased palmitoylation of barttin as assessed by both ABE assay (Fig. 1*C*) and radioactive labeling (Fig. S2*B*). Notably, knockdown of DHHC7 did not affect barttin expression (Fig. 1*C* and Fig. S2*B*).

To verify a possible involvement of DHHC3 in barttin palmitoylation, we knocked down this acyltransferase using specific shRNA. Although expression of this shRNA resulted in significant reduction of the amount of *DHHC3* transcript (Fig. 1*D*), we did not observe significant changes in barttin palmitoylation, even though the tendency to palmitoylation decrease was visible (Fig. 1*E*). When DHHC3 and DHHC7 were knocked down simultaneously, we obtained a significant decrease of barttin palmitoylation (Fig. 1*E*), which was greater than in the case of the single DHHC7 knockdown (Fig. 1*C*). Based on these results in combination with the results of radioactive labeling, which revealed the highest increase of barttin palmitoylation after co-expression with DHHC7 (Fig. S1), we decided to focus on DHHC7 as the presumably more potent PAT for barttin.

One of the central barttin functions is the proper localization of ClC-K channel proteins in the surface membrane of the nephron epithelium (4, 5). Therefore, we analyzed whether the overexpression or knockdown of DHHC7 can influence the subcellular distribution of barttin and ClC-K in MDCK II cells. YFP-ClC-Ka was expressed in MDCK II cells either alone (Fig. S3*A*) or together with barttin-CFP (Fig. S3*B*). In another set of experiments, barttin-CFP and YFP-ClC-Ka were co-expressed with DHHC7-GFP (Fig. S3*C*) or the shRNA against DHHC7 (Fig. S3*D*). The results confirmed the well-known barttin function of promoting ClC-Ka insertion into the plasma membrane (8). More importantly, manipulation of barttin palmitoylation via DHHC7 overexpression or knockdown did not result in any visible changes in the distribution of the ClC-Ka/barttin complex in MDCKII cells (Fig. S3, *C* and *D*).

Knockdown of DHHC7 reduces activation of hClC-Ka/barttin channels

Our previous results demonstrated that palmitoylation of barttin is mandatory for activation of the hClC-K/barttin channel complex, whereas the voltage dependence of activation and plasma membrane integration remained unchanged (8). Therefore, we hypothesized that modulation of barttin palmitoylation by overexpression or knockdown of DHHC7 influences the whole-cell current amplitudes of HEK293T cells expressing hClC-Ka/barttin.

Although the addition of scrambled shRNA or overexpression of DHHC7 did not substantially affect the current amplitudes, patch clamp experiments revealed a significant decrease in current amplitudes (>80% decrease) when shRNA against

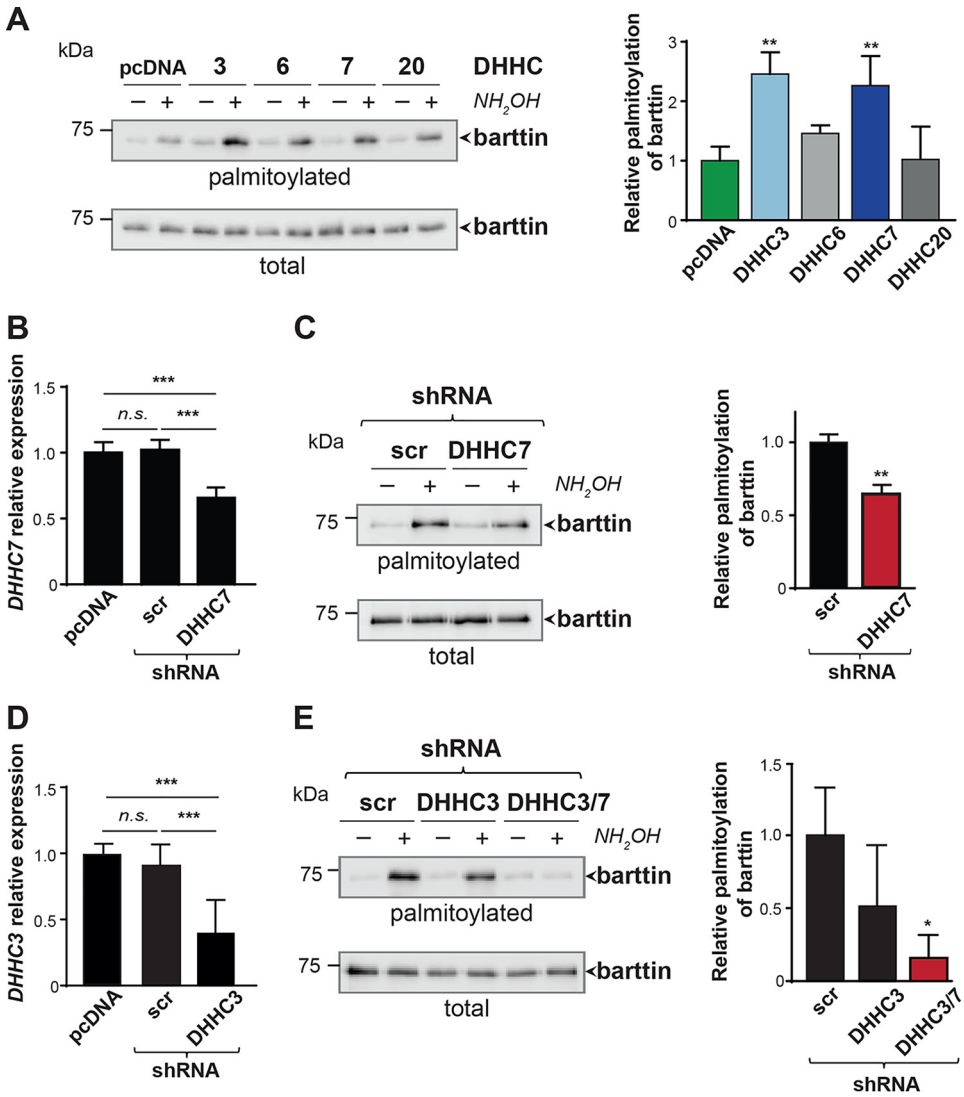

Figure 1. DHHC7 is an important barttin palmitoyl acyltransferase. *A*, HEK293T cells co-expressing barttin and the indicated DHHCs were analyzed by ABE. Representative blots are shown on the *left*, and quantifications of barttin palmitoylation after co-expression of DHHC3, DHHC6, DHHC7, and DHHC20 ($n = 3$) are shown on the *right* (see also Fig. S1). **, $p < 0.01$, one-way ANOVA; Dunnett's multiple-comparison test. *B* and *D*, bar graphs indicate the expression level of *DHHC7* mRNA ($n = 4$; *B*) or *DHHC3* mRNA ($n = 6$; *D*) in HEK293T cells after transfection with shRNA against DHHC7 or DHHC3, respectively. RT-qPCR analysis was evaluated by the $\Delta\Delta Ct$ method. ***, $p < 0.001$, one-way ANOVA, Tukey's multiple-comparison test. *C* and *E*, ABE analysis of barttin palmitoylation in HEK293T cells after knockdown of endogenous DHHC7 (*C*) or DHHC3 (*E*) by shRNA (*left panels*). Quantification is shown on the *right* (see also Fig. S2*A*). Western blots are representative of at least three independent experiments. **, $p < 0.01$, Student's *t* test (for *C*); one-way ANOVA, Dunnett's multiple-comparison test (for *E*). All data are shown as mean + S.D. (*error bars*).

DHHC7 was co-expressed together with barttin-CFP and mCherry-hClC-Ka (Fig. 2, *A–C*). As barttin expression levels were not affected by co-expression of DHHCs or shRNA (Fig. 1 and Figs. S1 and S2), the reduced current amplitudes could be the result of decreased single channel conductance, reduced open probabilities, or a reduced number of active channels in the cell membrane. Stationary noise analysis was performed to define these parameters based on the variance of whole-cell currents. The steady-state current variance (σ^2) was measured for voltages between −5 and −245 mV, normalized by the product of the steady-state current amplitude (I) and the electrical driving force $V\text{-}Vrev$ and plotted against the whole-cell conductance $I/(V\text{-}Vrev)$ (Fig. 2*D*). A linear regression line revealed the single-pore conductance gCl ($= i/(V\text{-}Vrev)$) as the y axis intercept (Fig. 2*E*), and the number of active channels in the cell membrane as negative inverse slope ($n = -1/\text{slope}$). Furthermore, these values allow calculation of the absolute open probabilities of active channels (Fig. 2*F*). The reduced barttin palmitoylation mediated by the knockdown of DHHC7 affected neither the single channel conductance nor the voltage dependence of absolute open probabilities. The maximum and minimum open probabilities and mid-voltage of activation (*Vmid*) were comparable for controls, overexpressed DHHC7, and diminished DHHC7 (Fig. 2, *F* and *G*). Because single-channel conductance and open probabilities were seemingly not altered, these results suggest that the current reduction obtained after DHHC7 knockdown most likely resulted from a reduced number of active channels (N) in the plasma membrane, as also indicated by the steep regression line for shDHHC7 in the representative noise analysis (Fig. 2*D*, *red symbols*).

To verify whether the decreased channel activation after DHHC7 knockdown can be mediated by decreased surface

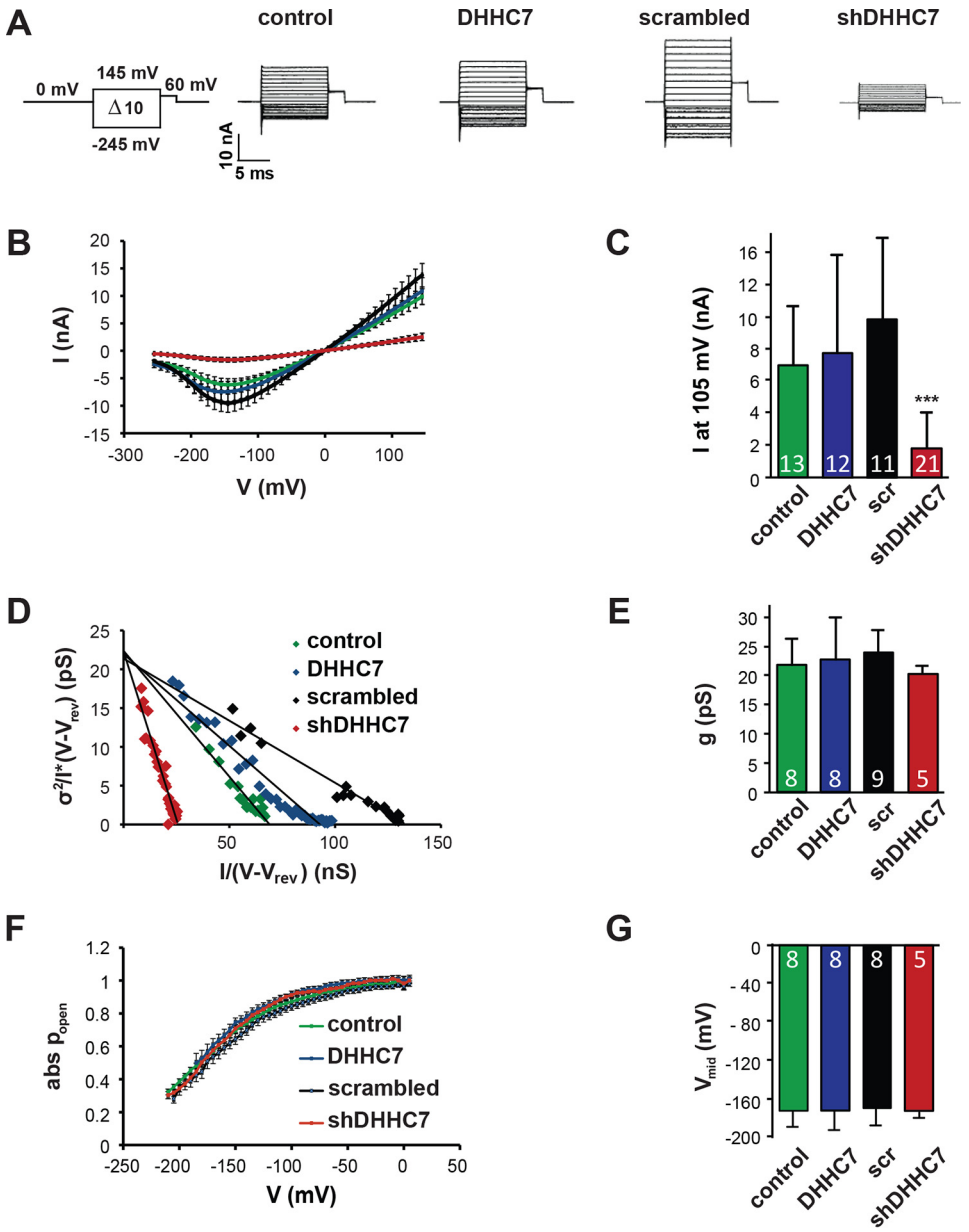

Figure 2. Knockdown of DHHC7 decreases macroscopic ClC-Ka/barttin currents. *A*, voltage protocol and representative whole-cell current recordings from HEK293T cells expressing hClC-Ka/barttin channels under varying conditions of DHHC7 expression: *control*, presence of endogenous DHHC7; *DHHC7*, overexpression of DHHC7; *shRNA*, partial knockdown of DHHC7 (shRNA against a scrambled target sequence (*scr*) served as control). *B*, voltage dependence of hClC-Ka/barttin currents under varying conditions of DHHC7 expression. *C*, comparison of mean current amplitudes at 105 mV. *D–G*, stationary noise analysis of hClC-Ka/barttin currents. *D*, representative plot of the current variance σ^2, normalized to the product of the mean current amplitude (*I*) and the electrical driving force (*V-Vrev*), *versus* the macroscopic conductance (*I*/(*V-Vrev*)). A linear regression provides the single channel conductance (*gCl*) as *y* axis intercept and the number of active channels as inverse slope. *E*, mean values of single-channel conductance (*gCl*). *F*, voltage dependence of absolute open probabilities of hClC-Ka/barttin channels. *G*, mean values of V_{mid}, the voltage of half-maximal activation of hClC-Ka/barttin. *B* and *F*, all data are mean ± S.E.M. (*error bars*); *C*, *E*, *G*, all data are mean + S.D. (*error bars*); *n* is indicated in the bar graphs; ***, $p \leq 0.001$, Student's *t* test.

expression of ClC-K/barttin complexes, we performed surface biotinylation experiments (Fig. 3). Results of this analysis revealed that the amount of ClC-K channels as well as barttin in the plasma membrane were not affected after selective knockdown of DHHC7, when compared with cells transfected with pcDNA3.1 or scrambled shRNA. Altogether, the above-mentioned results (*i.e.* Figs. 2 and 3 and Fig. S3) are in line with our previous observation that nonpalmitoylated barttin did not reduce surface membrane insertion of ClC-K/barttin, but selectively impaired activation of the channel complex (8).

Characterization of the kidney morphology of Zdhhc7$^{-/-}$ mice

To investigate the impact of DHHC7 on barttin palmitoylation *in vivo*, we established a *Zdhhc7*$^{-/-}$ mouse line (27). We previously demonstrated that *Zdhhc7*$^{-/-}$ mice possess a normal range of sensory and motor activity and reproduction. We did not observe any signs of burden or stress under standard housing conditions. Kidney slices from *Zdhhc7*$^{-/-}$ and WT mice (P90, males, littermates) were analyzed for possible pathological changes, including interstitial fibrosis, sclerotic changes in

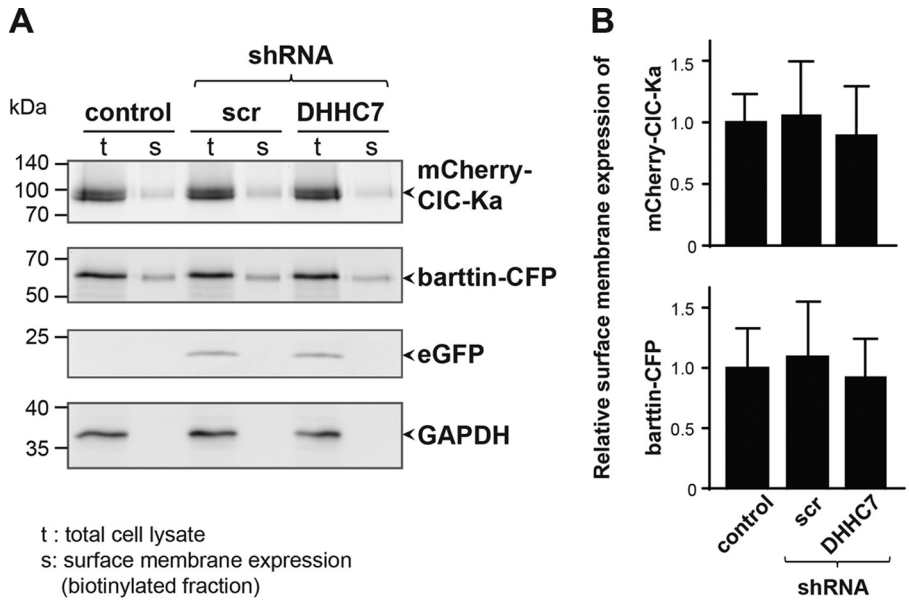

Figure 3. Knockdown of endogenous DHHC7 induces no changes in ClC-Ka/barttin distribution. *A*, fluorescent scans of SDS-polyacrylamide gels depicting mCherry-ClC-Ka, barttin-CFP, and eGFP (used as a cytosolic reporter for the shRNA transfection) in whole-cell lysates (*t*) and the biotinylated protein fractions of the surface membrane (*s*) of HEK293T cells that additionally co-expressed either no shRNA (empty pcDNA vector) or scrambled shRNA (*scr*) or shRNA against DHHC7. *Bottom*, Western blot analysis using anti-GAPDH antibodies excludes contamination of the surface membrane fraction by cytosolic proteins. *B*, quantification of the relative expression of mCherry-ClC-Ka and barttin-CFP in the surface membrane. Fluorescence intensities in the surface membrane fractions were normalized by the corresponding intensities of proteins in the whole-cell lysates. There was no statistically significant difference between experimental conditions as tested by one-way ANOVA. Data are presented as means + S.D. (*error bars*) ($n = 3$).

glomeruli, hyperplasia of the juxtaglomerular apparatus, and dilated or atrophic tubules. As shown in Fig. S4, no apparent morphological differences were detected in the renal cortex or outer or inner medulla of *Zdhhc7*$^{-/-}$ mice.

Next, we compared the distribution of ClC-K/barttin channels within a nephron. For detection of the ClC-K channels, we applied rabbit polyclonal antibody from Alomone Labs, which has long been accepted as a highly specific and fairly unambiguous tool for visualization of the ClC-K channel both *in vitro* and *in vivo* (28–30). For visualization of barttin, we used the goat polyclonal antibody sc-49611 from Santa Cruz Biotechnology, Inc. (Heidelberg, Germany). This antibody was characterized in detail in our previous study (8). The specificity of both antibodies was verified using corresponding blocking peptides, which are available from the manufacturers. Under physiological conditions, the ClC-K/barttin complex is highly expressed in the distal convolute tubule (DCT), in medullar thick (mTAL) and thin ascending limb (mTL) of the loop of Henle, and in intercalated cells of the collecting duct (31, 32). Immunofluorescence analysis of kidney slices from adult mice (P90, males, littermates) revealed similar basolateral localization of barttin in DCT, mTAL, and α-intercalated cells of the collecting duct in both WT and *Zdhhc7*$^{-/-}$ mice (Fig. S5, *A* and *B*). In line with previous observations (31), barttin and ClC-K channels were co-localized on both the apical and basolateral sites of the mTL in WT and *Zdhhc7*$^{-/-}$ mice (Fig. S5*A*).

Barttin is a DHHC7 substrate in mouse kidney

To investigate whether knocking out *Zdhhc7* affects barttin palmitoylation *in vivo*, we compared barttin palmitoylation levels in the kidneys of WT and *Zdhhc7*$^{-/-}$ mice at different developmental stages. Palmitoylation analysis performed by ABE revealed a significant reduction in barttin palmitoylation in the kidneys of *Zdhhc7*$^{-/-}$ mice compared with WT animals, whereas barttin expression was not affected in newborn (P0) or adult (P90) mice (Fig. 4, *A* and *B*). Importantly, the global palmitoylation patterns in the kidneys of *Zdhhc7*$^{-/-}$ animals were not changed (Fig. 4*C*).

To further verify the role of DHHC7 in barttin palmitoylation in the mouse kidney, we applied a high-throughput PANIMoni proteomics technique that enables identification of *S*-palmitoylated cysteine residues in complex biological mixtures (33). Using this approach in combination with MS protein identification, we confirmed barttin palmitoylation in the mouse kidney of WT mice (Fig. 5 (*A* and *B*) and Table S1). Quantitative analysis of the palmitoylomics data from the kidneys of WT and *Zdhhc7*$^{-/-}$ mice demonstrated that knocking out DHHC7 led to a significant decrease in barttin palmitoylation to 68 ± 25% (Fig. 5*A*). This is similar to the results obtained by ABE (Fig. 4) and confirms that barttin is a physiological substrate for DHHC7 in mouse kidney.

In addition, MS-based PANIMoni analysis of palmitoylated peptides revealed two differently palmitoylated barttin populations: one containing barttin palmitoylated on both Cys-54 and Cys-56 and one in which only Cys-54 undergoes palmitoylation (Fig. 5, *B* and *C*). Notably, we were not able to detect peptides with a single palmitoylated Cys-56, suggesting that this cysteine residue can only be palmitoylated in combination with Cys-54. The existence of two different populations of palmitoylated barttin was confirmed by the acyl-PEGyl exchange gel shift approach (Fig. 5*D*).

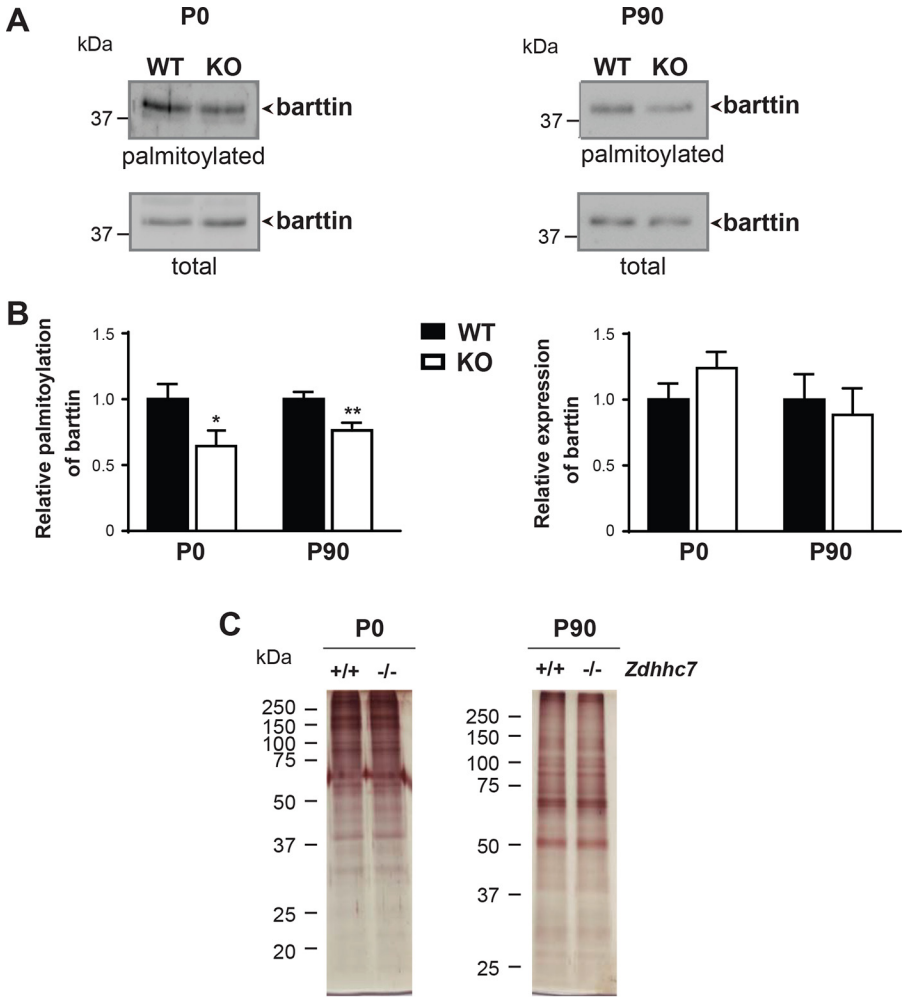

Figure 4. Palmitoylation of barttin is decreased in the kidneys of *Zdhhc7*$^{-/-}$ mice (ABE). *A* and *B*, kidney tissues isolated from the newborn (P0) and adult (P90) *Zdhhc7*$^{+/+}$ (*WT*) ($n = 3$) and *Zdhhc7*$^{-/-}$ (*KO*) ($n = 3$) mice were collected for ABE analysis. Representative Western blots are shown in *A* following by quantification (*B*). *, $p < 0.05$; **, $p < 0.01$, Student's *t* test. *Bars*, means + S.D. (*error bars*). *C*, representative silver staining demonstrating a global protein palmitoylation in mouse kidneys from newborn (P0) and adult (P90) *Zdhhc7*$^{+/+}$ and *Zdhhc7*$^{-/-}$ mice.

Zdhhc7$^{-/-}$ *mice develop a Bartter-like phenotype with a low-salt diet*

Having demonstrated the importance of barttin palmitoylation for ClC-K channel activation (Fig. 2) and decreased barttin palmitoylation in the kidneys of *Zdhhc7*$^{-/-}$ mice (Figs. 4 and 5), we investigated whether *Zdhhc7*$^{-/-}$ animals develop a Bartter-like phenotype. When fed a normal diet, *Zdhhc7*$^{-/-}$ mice did not present any apparent phenotype in gross physical appearance, body weight, kidney morphology, or laboratory measurements in urine or blood (Table 1 and Fig. 6 (*A* and *B*)). However, when the mice were fed a low-salt diet for 12 days, they developed a salt-losing phenotype characterized by hyponatremia and mild metabolic alkalosis (Table 1 and Fig. 6 (*C* and *D*)). Interestingly, on the low-salt diet, the relative decrease in barttin palmitoylation was more pronounced in *Zdhhc7*$^{-/-}$ mice than the animals fed a normal diet (38 and 24%; Fig. 7, *A* and *B* and Fig. 4, *A* and *B*, respectively). Importantly, neither the level of barttin expression nor the global palmitoylation profile was affected by the low-salt diet (Fig. 7). More detailed analysis of barttin palmitoylation revealed that a low-salt diet boosts barttin palmitoylation, which is needed to facilitate the compensatory renal salt reabsorption by switching ClC-K channels into an active state, in the WT mice but not in *Zdhhc7*$^{-/-}$ mice (Fig. 7*B*). Thus, the decreased barttin palmitoylation results in hyponatremia and metabolic alkalosis in *Zdhhc7*$^{-/-}$ mice fed a low-salt diet.

Disease-causing R8L mutation impairs barttin palmitoylation

Similar systemic effects of a low-salt diet were previously reported for R8L barttin knock-in mice (34). The naturally occurring R8L mutation in *BSND* has been shown to be associated with BS Type IV in humans (2). Although this mutation does not affect the subcellular transport and plasma membrane localization of the ClC-K/barttin complex, the current amplitude of hClC-Ka channels was significantly decreased after co-expression of barttin R8L mutant compared with WT barttin (3). As co-expression of the palmitoylation-deficient barttin mutant (8) or knockdown of endogenous DHHC7 (Fig. 2 and Fig. 3) results in similar abrogation of ClC-Ka channel functions, we hypothesized that altered palmitoylation of the R8L barttin mutant may be the reason for its functional defect. Supporting this view, palmitoylation of R8L barttin heterologously expressed in HEK293T cells was significantly reduced to 43.4 ± 14.9% (Fig. 8, *A* and *B*).

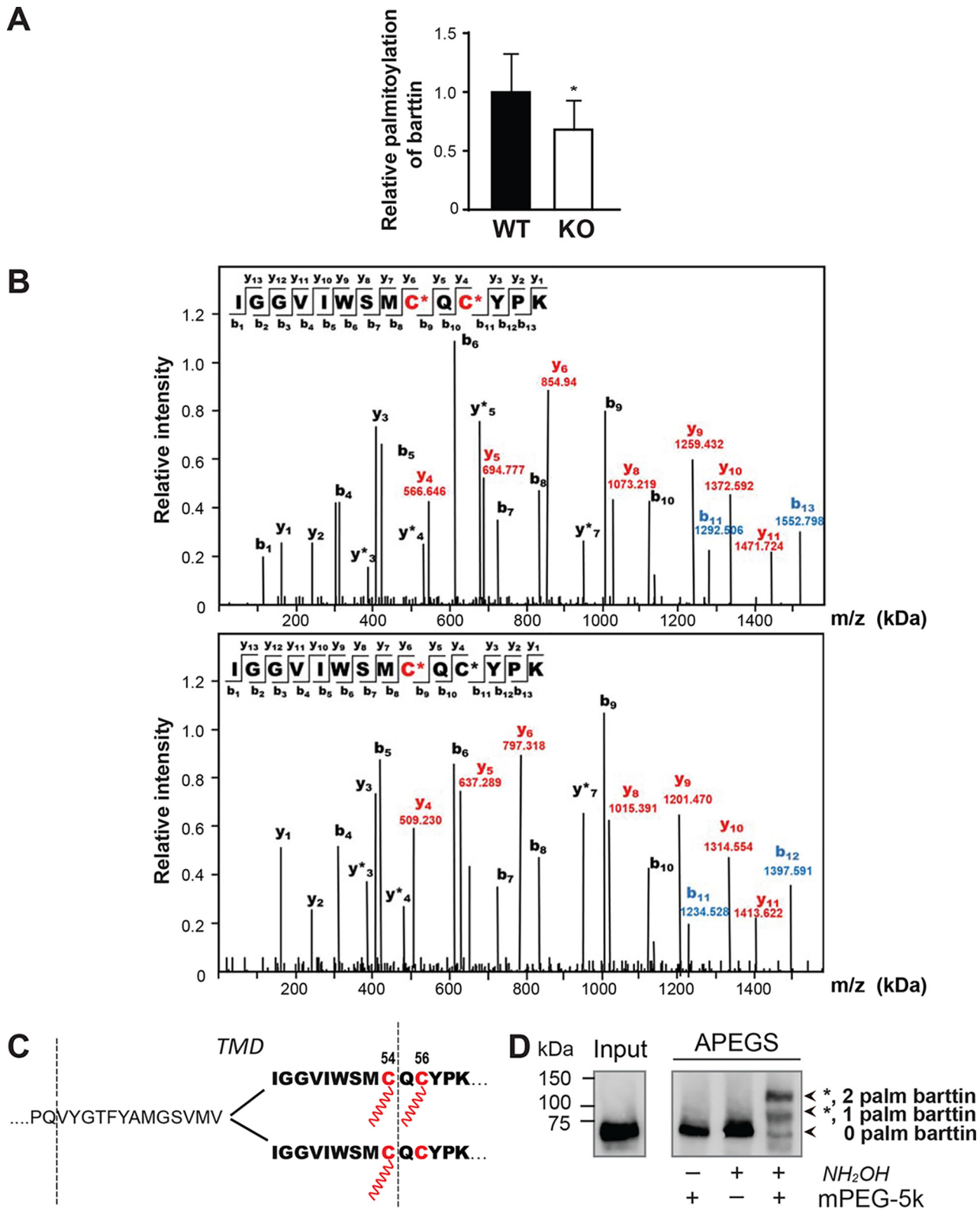

Figure 5. Palmitoylation of barttin is decreased in the kidneys of *Zdhhc7*$^{-/-}$ mice (palmitoylomics), where two differently palmitoylated barttin populations co-exist. *A*, kidney tissues isolated from adult (P90) *Zdhhc7*$^{+/+}$ (*WT*) ($n = 3$) and Zdhhc7$^{-/-}$ (*KO*) ($n = 3$) male mice were subjected to a quantitative palmitoylomics approach to evaluate the levels of barttin palmitoylation. *Bars*, means + S.D. (*error bars*); *, $p < 0.05$, Student's *t* test. *B*, PANIMoni MS-based analysis of palmitoylated peptides isolated from the mouse kidney. *Red-labeled peaks* in the spectrum correspond to matched y-ions, and *blue-labeled peaks* correspond to matched b-ions, which differentiate peptides with one and two modified cysteines. The number paired with each ion identification (*i.e.* b3, y7, etc.) indicates the number of amino acids present on N-terminal fragments for b-ions and C-terminal fragments for y-ions. Modified cysteines in the sequence are *marked* in *red* and indicated by *asterisks*. *C*, *schematic representation* of two palmitoylated barttin forms. Protein sequence is shown with a *single-letter code*. Palmitoylation sites (Cys-54 and Cys-56) are depicted in *red*. *TMD*, transmembrane domain. *D*, HEK293T cells transfected with barttin-CFP WT were lysed, subjected to APEGS, separated by SDS-PAGE, and analyzed by Western blotting. The number of PEGylation events is indicated by *asterisks*.

Table 1
Weights and blood parameters from *Zdhhc7*$^{+/+}$ (WT) and *Zdhhc7*$^{-/-}$ (KO) mice fed at a normal diet or subjected to a low-salt diet
Data represent mean ± S.D. *n* is indicated in parentheses.

Parameters	Standard diet		Low-salt diet	
	WT	KO	WT	KO
Weight, g	29.06 ± 0.37 (10)	29.61 ± 0.79 (9)	30.36 ± 0.38 (10)	30.66 ± 0.81 (9)[a]
Blood Na, mmol/liter	146.20 ± 0.80 (5)	145.80 ± 0.45 (5)	141.60 ± 0.40 (10)	137.78 ± 1.39 (9)[b]
Blood K, mmol/liter	3.94 ± 0.081 (5)	3.96 ± 0.075 (5)	3.72 ± 0.081 (10)	3.81 ± 0.072 (9)[a]
Blood Cl, mmol/liter	112.00 ± 0.84 (5)	110.80 ± 0.86 (5)	104.80 ± 1.44 (10)	104.44 ± 1.13 (9)[a]
Blood pH	7.247 ± 0.011 (5)	7.225 ± 0.019 (5)	7.323 ± 0.012 (10)	7.363 ± 0.017 (9)[a]
Blood HCO_3^-, mmol/liter	18.14 ± 0.67 (5)	17.44 ± 0.48 (5)	23.88 ± 0.62 (10)	25.28 ± 0.68 (9)[a]

[a] Not significant.
[b] $p < 0.05$, Tukey's multiple-comparison test.

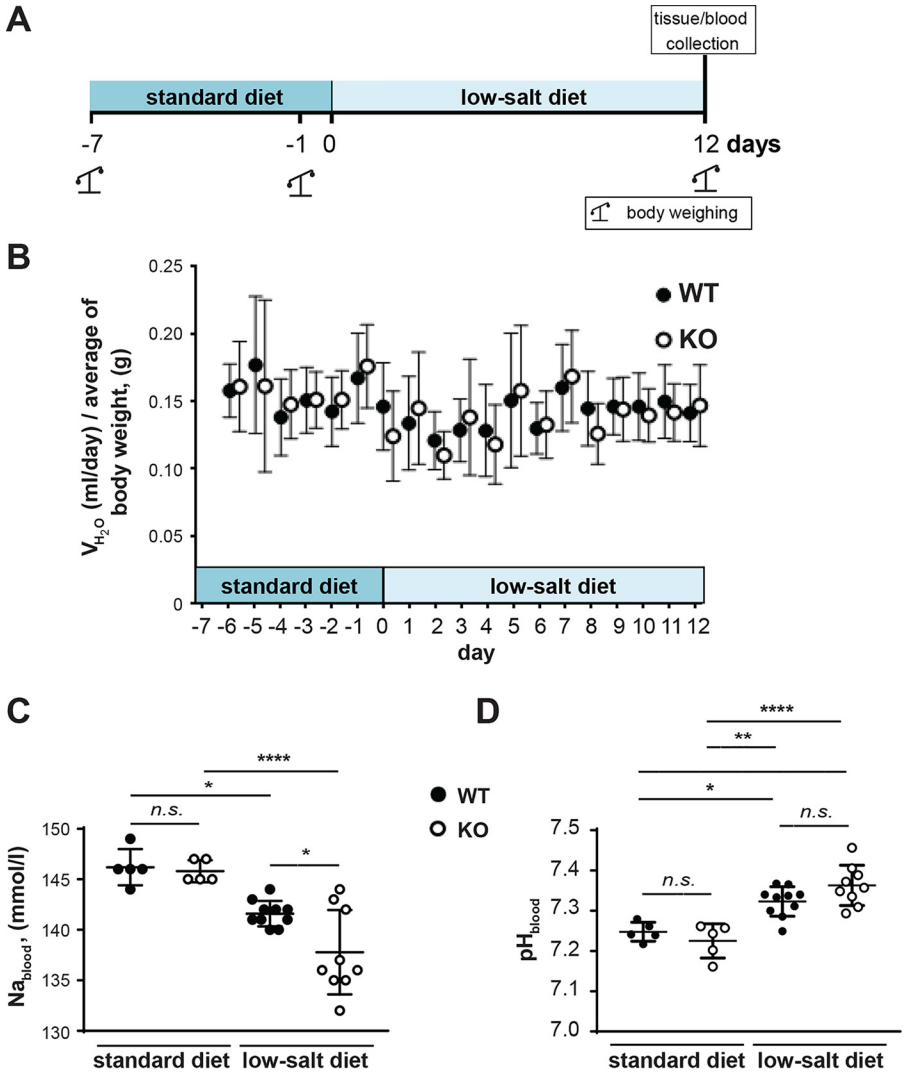

Figure 6. Zdhhc7$^{-/-}$ mice develop a salt-losing phenotype under a low-salt diet. *A*, *schematic diagram* of experimental design for the low-salt diet experiments. *B*, water intake in WT and *Zdhhc7*$^{-/-}$ mice during the experiment. Water intake was normalized to the body weight (WT, standard diet $n = 9$, low-salt diet $n = 11$; *Zdhhc7*$^{-/-}$, standard diet $n = 7$, low-salt diet $n = 10$). All data are mean ± S.D. *C*, blood sodium concentration in *Zdhhc7*$^{+/+}$ (*WT*) and *Zdhhc7*$^{-/-}$ (*KO*) mice was measured after feeding a normal (standard diet) and low-salt diet for 12 days. Data represent means ± S.D. (*error bars*) (*n* is indicated in *dots*). *, $p < 0.05$; ****, $p < 0.0001$, Tukey's multiple-comparison test. Upon low-salt diet, *Zdhhc7*$^{-/-}$ animals developed a salt-losing phenotype characterized by hyponatremia (Table 1). *D*, analysis of blood pH in animals subjected to a standard and low-salt diet. *, $p < 0.05$; **, $p < 0.01$; ***, $p < 0.001$; ****, $p < 0.0001$, one-way ANOVA. *n.s.*, not significant. All data are mean ± S.D.

Discussion

We previously showed that barttin is palmitoylated at Cys-54 and Cys-56, and palmitoylation is essential for activation of the ClC-K/barttin channel complex (8). In the present study, we identified DHHC3 and DHHC7 as the cognate palmitoylating enzymes and found that reduced DHHC7 expression leads to attenuated barttin palmitoylation status. Because DHHC3 and DHHC7 belong to the same subfamily of PATs with high sequence homology within the cysteine-rich domain (25), it is not surprising that these enzymes may have overlapping substrates. On the other hand, *in vivo* studies have revealed distinct substrate specificity for these PATs in the mouse brain (35).

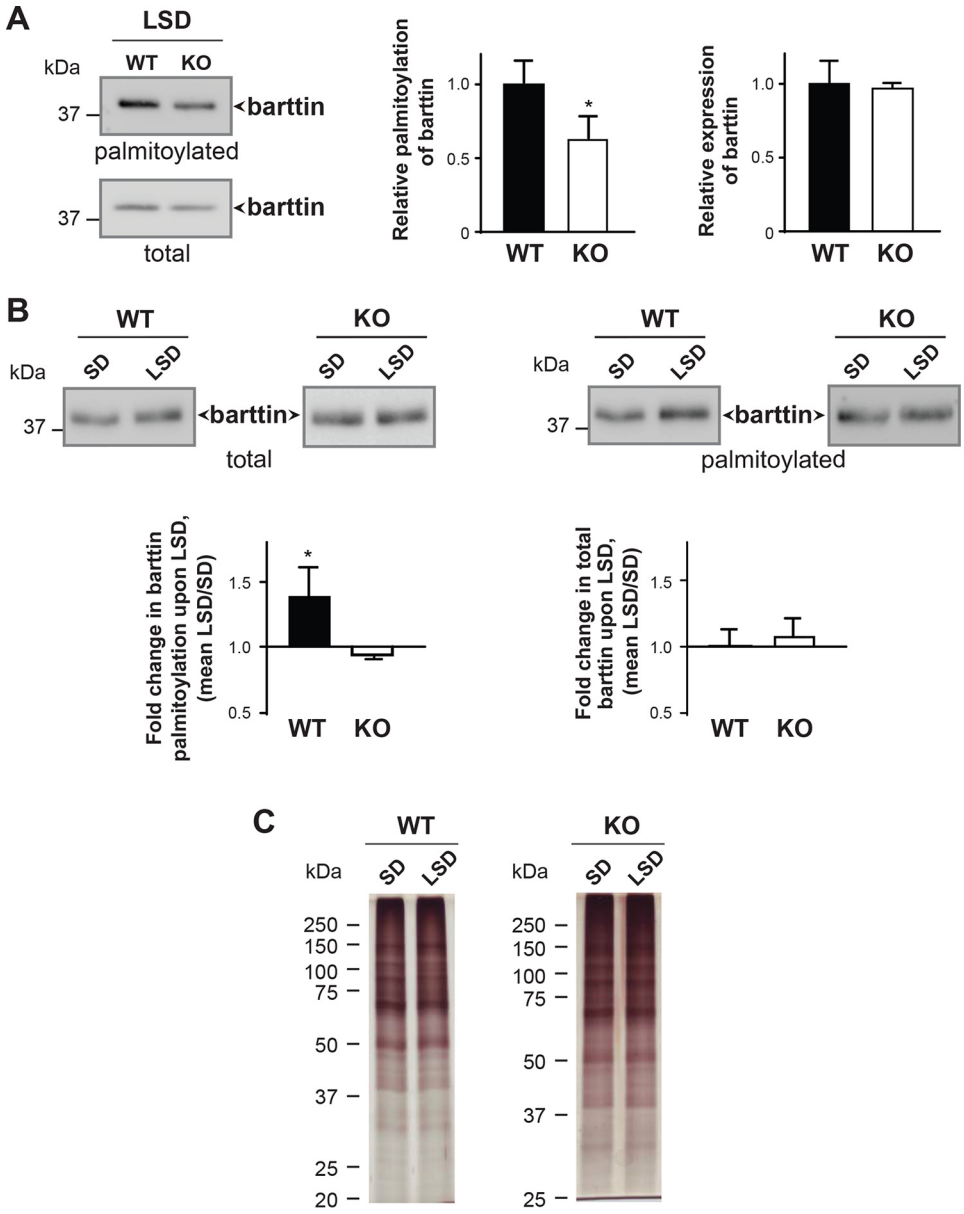

Figure 7. Palmitoylation of barttin is affected in salt-losing phenotype under a low-salt diet. *A*, representative image of barttin palmitoylation in kidneys from WT and *Zdhhc7*$^{-/-}$ mice subjected to a low-salt diet as assessed by ABE followed by SDS-PAGE and Western blotting (*left*). Relative palmitoylation and expression levels of barttin are shown on the *right*. Data represent means + S.D. (*error bars*) ($n = 3$). *, $p < 0.05$, Student's *t* test. *B*, direct comparison of barttin palmitoylation and expression in kidney of WT and *Zdhhc7*$^{-/-}$ mice under standard diet (*SD*) and low-salt diet (*LSD*). Representative Western blotting images after ABE are shown on the *top*. Quantification of relative changes in palmitoylation and expression between standard diet and low-salt diet for WT and *Zdhhc7*$^{-/-}$ is shown *below* in bar graphs. Data represent means + S.D. ($n = 3$). *, $p < 0.05$, Student's *t* test. *C*, representative silver staining demonstrating a global protein palmitoylation in mouse kidneys from *Zdhhc7*$^{+/+}$ (WT) and *Zdhhc7*$^{-/-}$ (KO) mice after standard diet and low-salt diet.

Knockdown experiments in cultured cells demonstrated that the presence of endogenous DHHC3 is not enough to fully compensate for DHHC7 deficiency. These findings suggest that DHHC7 is an important regulator of barttin palmitoylation.

Our electrophysiological experiments revealed that knocking down endogenous DHHC7 leads to impaired barttin palmitoylation, which significantly reduces macroscopic ClC-K current amplitudes. In combination with the observation that DHHC7 knockdown does not alter the subcellular distribution of the ClC-K/barttin complex, this finding suggests that hClC-K channels remain inactive in complex with nonpalmitoylated barttin, whereas barttin palmitoylation can switch channels to an active state. Decreased barttin palmitoylation mediated by the DHHC7 knockdown appears to promote long-lasting closure of ClC-K channels. When dwell times for being trapped in such closed states are longer than applied voltage steps in noise analyses, an apparent reduction of counted channels (N) is observed. Active channels, however, have unaltered absolute open probabilities. This notion is in agreement with previous observations of transiently transfected HEK293T cells (8) and native renal epithelia (36) that indicated the presence of large numbers of well-integrated but inactive ClC-K channels in the plasma membrane.

The presence of palmitate groups on barttin might have several functional consequences. Palmitoylation can be involved in the creation of a direct hydrophobic interface between barttin

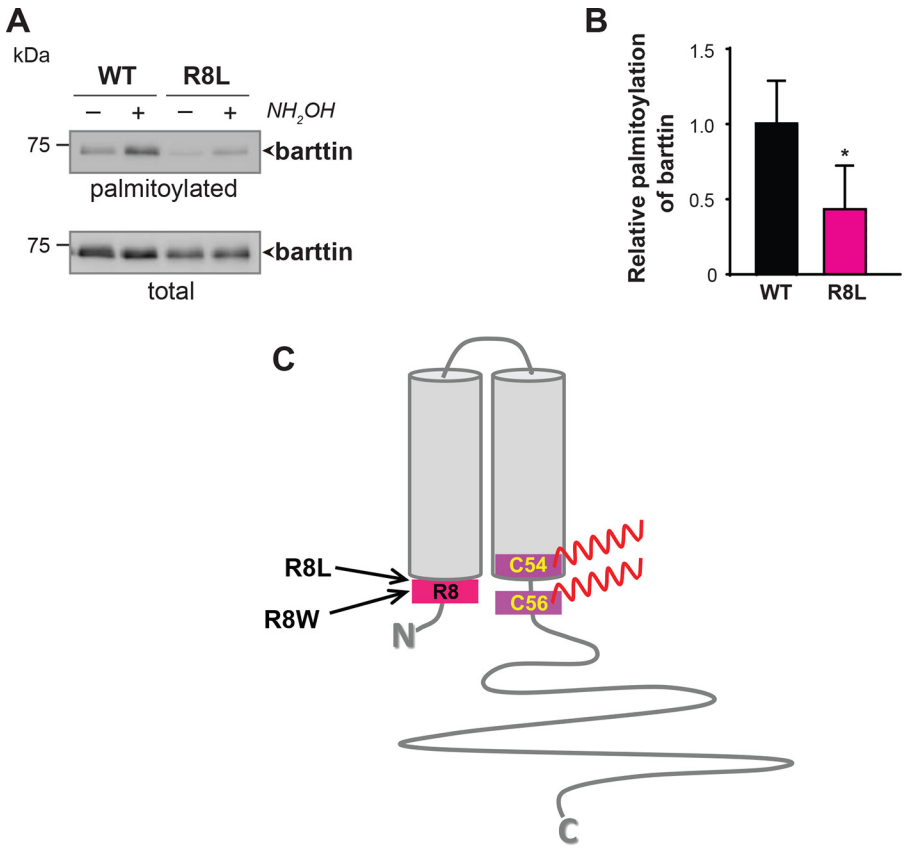

Figure 8. Disease-causing barttin mutation R8L affects palmitoylation of barttin. *A*, representative image from ABE palmitoylation assay followed by SDS-PAGE and Western blotting for WT and R8L barttin mutant. *B*, relative palmitoylation levels of WT and R8L barttin mutant. Data are shown as means + S.D. (*error bars*) ($n = 4$). *, $p < 0.05$. Student's *t* test. *C*, putative topology of barttin with positions of Arg-8, Cys-54, and Cys-56.

and the plasma membrane, which can adjust the orientation of barttin within the lipid bilayer and facilitate specific interaction and conformational changes within the ClC-K channel itself, particularly within its B- and J-helices (37). A similar mechanism has been proposed for human voltage-dependent K^+ channels (38). In addition, through direct interaction with the membrane lipids, the palmitate groups of barttin can change the lipid membrane environment surrounding the ClC-K channel and/or create membrane dipoles, which in turn influence the functional activity of the ClC-K/barttin channels (39).

Intriguingly, although reduction of barttin palmitoylation strongly affects ClC-K channel activity, increased barttin palmitoylation evoked by the overexpression of DHHC7 did not influence the ClC-K/barttin surface expression in MDCKII cells and channel properties. One possible explanation is that, because of overexpression, a supra-optimal amount of palmitoylated barttin with a higher affinity for the ClC-K channel participates in ClC-K/barttin complex formation, leading to functional "saturation." Conceivable for the heterologous system, this scenario seems not to be relevant for the *in vivo* conditions. In our previous study, we measured a significant increase in barttin palmitoylation in mouse kidney upon water deprivation (8). Similar effects were observed in the present study in the kidneys of mice subjected to a low-salt diet. In both cases, increased barttin palmitoylation in the ClC-K/barttin channel may modify chloride conductance in the thin and thick ascending limb of the loop of Henle and facilitate urinary concentration and reduce water excretion. Thus, dynamic palmitoylation of barttin in the kidney could represent a mechanism for fine-tuning ClC-K/barttin channel function.

To investigate the physiological importance of barttin palmitoylation in ClC-K/barttin function *in vivo*, we generated *Zdhhc7*$^{-/-}$ mice. In these animals, palmitoylation of barttin was significantly decreased throughout their entire life span, further confirming DHHC7 as an important barttin palmitoyl acyltransferase. On the other hand, *Zdhhc7*$^{-/-}$ mice were indistinguishable from WT mice in terms of general health, motor and sensory activity, reflexes, and reproduction. We also did not find any morphological and histological differences in the renal cortex or outer or inner medulla. Moreover, barttin and ClC-K channel expression, distribution, and co-localization within the mTAL and DCT were not affected. These data suggest that knocking out *Zdhhc7* (consequently decreasing barttin palmitoylation) has no critical consequences for normal kidney function under physiological conditions. However, when *Zdhhc7*$^{-/-}$ animals were fed a low-salt diet, they developed hyponatremia and mild metabolic alkalosis, symptoms characteristic of human BS Type IV with late onset (40). Our experimental data suggest that decreased barttin palmitoylation can be the main reason for a missing compensatory effect of the salt-losing phenotype in *Zdhhc7*$^{-/-}$ mice: As part of the compensatory facilitation of ClC-K channel activity, we achieved increased barttin palmitoylation in WT mice, and it was completely absent in *Zdhhc7*$^{-/-}$ mice.

Interestingly, a similar phenotype (*i.e.* hyponatremia and mild metabolic alkalosis manifested with a low-salt diet) was obtained in R8L knock-in mice (34). The R8L mutation was identified in human BS Type IV (2) and was previously shown to eliminate the function of ClC-K/barttin channels in MDCK II cells (3). In the latter study, authors showed that R8L modifies intracellular distribution of barttin and ClC-Kb but does not prevent their surface membrane insertion. Moreover, the authors used concatamers of hClC-1 and hClC-Kb, which can be transported to the plasma membrane without barttin, to explicitly show that the ClC-K subunit could not be switched to an active conformation by the R8L barttin mutant (3). Results obtained from the knock-in mouse model of Nomura *et al.* (34) tend in the same direction: The authors show reduced or unclear surface membrane staining of R8L barttin in renal epithelia of the mice. However, in contrast to their Neo/Neo mouse that lacks barttin expression, the R8L knock-in mouse displays no phenotype under normal diet and only a mild phenotype with affected urine or blood data under low-salt diet. These results clearly indicate that ClC-K and R8L barttin must be inserted in the surface membrane of renal epithelia of these mice.

Lack of proper activation of the ClC-K channels has also been described for R8W, another naturally occurring mutation in *BSND* that is associated with BS Type IV in humans (2). These data suggest that the major pathogenic consequence of Arg-8 mutations is their inability to functionally activate ClC-K. Searching for underlying mechanisms, we found that palmitoylation of both R8L (this study) and R8W (8) mutants is significantly reduced. These combined results suggest that the negative effects of R8L and R8W mutations on barttin functions may be explained, at least in part, by changes in their palmitoylation. Arginine at position 8 is proposed to be localized within the first intracellular barttin domain very close to the cytosolic membrane border (2) (Fig. 8*C*) and can thus be part of the structural consensus recognized by the acyl-enzyme intermediate of DHHC7 (41).

Taken together, in the present study, we identified DHHC7 as a main palmitoyl acyltransferase for barttin and demonstrated an important role of DHHC7-mediated barttin palmitoylation in the renal adaptation to salt deprivation in mice. Thus, *Zdhhc7*$^{-/-}$ mice may be a suitable model for investigating chronic hyponatremia caused by the renal failure associated with BS Type IV. Moreover, targeting DHHC7 activity may allow the development of novel therapeutic strategies for antihypertensive treatment.

Experimental procedures

Ethical statement

This study was conducted in accordance with the German animal protection law and with the European Directive 2010/63/EU. All experiments were approved by the local institutional animal care and research advisory committee and permitted by the Lower Saxony State Office for Consumer Protection and Food Safety (LAVES; file number 16/2230).

Cell culture and transfection

For experiments *in vitro*, human embryonic kidney cells (HEK293T) and Madin–Darby canine kidney cells (MDCK II) were handled as described previously (8). For electrophysiological experiments, HEK293T cells were first transfected with cDNA encoding DHHC7, shRNA against DHHC7 or scrambled, or an empty pcDNA3.1(+) vector. The second transfection step with cDNA encoding mCherry-hClC-Ka and barttin-CFP followed after 24 h. Twelve hours after the second transfection, cells expressing barttin-CFP and mCherry-hClC-Ka were analyzed as described previously (8).

Cloning and constructs

Hemagglutinin (HA)-tagged DHHCs (DHHC1 to -23) and DHHC7-GFP subcloned into pEF-BOS-HA and pEGFP-C1 plasmids, respectively, were a kind gift from Masaki Fukata. To knock down the endogenous DHHC7 or DHHC3 in HEK293T cells, shRNA against human DHHC7 (5′-GGATATCAACAGCTCATCT) binding to the noncoding region or shRNA against human DHHC3 (5′-GTACTTCGTCCTGTTTACA) binding to the coding region as well as scrambled shRNA (5′-AACAGTCGCGTTTGCGACTGG) were cloned into pSuper.gfp/neo vector (Oligoengine). The shRNA efficacy against DHHC7 or DHHC3 was tested in HEK293T cells by qPCR using primer probe Hs00938102_m1 or Hs00213209_m1 from the TaqMan gene expression assay, respectively. For quantification, the $\Delta\Delta C_T$ method was used (Applied Biosystems). Clones for YFP-hClC-Ka and R8L barttin were described before (3, 8).

Antibodies

For immunodetection, the following primary antibodies were used: anti-GFP (HRP) (LifeSpan BioScience, #LS-C50850), anti-GFP (GeneTex, #GTX26556), anti-Biotin (HRP) (Sigma, #A4541), anti-HA (HRP) (Roche Applied Science, #12013819001), and anti-barttin (Santa Cruz Biotechnology, #sc-49611). Secondary antibodies donkey-anti-goat IgG-HRP and goat anti-rabbit IgG-HRP were from Santa Cruz Biotechnology and Thermo Scientific, respectively. The intensity of protein bands after Western blots was quantified using ImageQuant™ software (GE Healthcare).

Radioactive labeling with [9,10-^{3}H(N)]palmitic acid

HEK293T cells were transfected with plasmid encoding human barttin-CFP together with individual HA-tagged palmitoyl acyltransferases (DHHC1 to -23). Twenty-four hours after transfection, cells were labeled with 300 μCi/ml [9,10-^{3}H(N)]palmitic acid (American Radiolabeled Chemicals, Inc.) for 2 h. Expression of barttin-CFP was detected by fluorescence scan of SDS-polyacrylamide gels. The amount of radioactive labeled barttin-CFP was visualized by autoradiography (exposures for 1 week). Expression of HA-DHHCs was visualized by Western blotting using anti-HA (HRP) antibody.

ABE and APEGS assays

The ABE method was used as described previously (8). The palmitoylation level of barttin was calculated by sum of replicates as described previously (42). To address the stoichiometry

of barttin palmitoylation, we made use of a recently developed method called acyl-PEGyl exchange gel shift (APEGS) (43). Briefly, HEK293T cells transfected with barttin-CFP were lysed, and free thiol groups were blocked using 40 mM *N*-ethylmaleimide. After treatment with 1.3 M hydroxylamine (NH_2OH) or 1.3 M Tris (pH 7.0), samples were incubated with 20 mM poly(ethylene glycol) methyl ether maleimide (5 kDa) or 20 mM *N*-ethylmaleimide. Finally, lysates were subjected to SDS-PAGE and Western blotting.

Electrophysiology

The whole-cell patch clamp recordings of HEK293T cells were performed from transiently transfected HEK293T cells as described previously (8). We performed stationary noise analyses as described before (8) to determine absolute open probabilities, single-channel conductance, and the number of active channels (N) from the variance (σ^2) of whole-cell currents. Plotting the variance normalized by the product of the steady-state current amplitude (I) and the electrical driving force (V-$Vrev$) *versus* the whole-cell conductance $I/(V\text{-}Vrev)$ reveals a linear relation with the single-channel conductance ($i/(V\text{-}Vrev)$) as the y axis intercept and the number of active channels as the negative inverse slope of the regression line.

$$\frac{\sigma^2}{I \cdot (V - Vrev)} = \frac{i}{(V - Vrev)} - \frac{1}{N} \cdot \frac{I}{(V - Vrev)} \quad \text{(Eq. 1)}$$

The absolute channel open probability (P) was subsequently determined by $P = I/(i{\cdot}N)$.

Biochemical analysis of ClC-Ka/barttin surface membrane insertion

Plasma membrane expression of ClC-Ka/barttin complexes in the presence of empty pcDNA3.1(+) vector, scrambled shRNA, or shRNA against DHHC7 was investigated using HEK293T cells. Twenty-four hours after transfection, cells were exposed to 0.375 mg of biotin (EZ-link sulfo-NHS-SS-biotin, Thermo Fisher Scientific) for 30 min. The biotinylation process was terminated by washing the cells with 10 mM glycine/PBS for 20 min followed by cell lysis with radioimmune precipitation assay buffer (100 mM NaCl, 20 mM HEPES, 1 mM sodium orthovanadate, 1 mM NaF, 1 mM EDTA, 1% SDS, 1% deoxycholate, 1% protease inhibitor mix, pH 7.4). After purification via NeutrAvidin affinity chromatography (High Capacity NeutrAvidin agarose, Thermo Fisher Scientific), biotinylated proteins were eluted by 2× Laemmli sample buffer. Subsequently, samples of total cell lysate as well as biotinylated protein fraction were electrophoresed on 12% SDS-polyacrylamide gels and scanned for fluorescent bands of mCherry-ClC-Ka, barttin-CFP, and GFP (+ shRNA scrambled/DHHC7). To ensure exclusive biotinylation of surface membrane proteins, Western blotting was performed with antibodies detecting GAPDH (primary antibody, GAPDH (A-3), sc-137179 (Santa Cruz Biotechnology); secondary antibody, rabbit anti-mouse IgG Fc, horseradish peroxidase conjugate (Thermo Fisher Scientific)).

Palmitoylomics

To identify specific sites of palmitoylated proteins in mouse kidneys, the PANIMoni method was used (33). Obtained after ABE, biotinylated protein lysates were digested using sequencing-grade modified trypsin (Promega V 5111) for 16 h at 37 °C. Digestion was terminated using protease inhibitor mixture (Complete, Roche Applied Science). The tryptic peptide mixture was incubated with 100 μl of neutravidin beads (Amersham Biosciences) at room temperature for 1 h. The neutravidin beads were washed five times in 1 ml of wash buffer. Neutravidin-bound peptides were eluted with 150 μl of elution buffer (25 mM NH_4CO_3 (pH 8.2) and 5 mM tris(2-carboxyethyl)phosphine (Sigma–Aldrich) and concentrated in a SpeedVac. TFA was added to the peptide solution to achieve a final concentration of 0.1%. The samples were analyzed using a Nano-Acquity (Waters) LC system and an Orbitrap Velos mass spectrometer (Thermo Electron Corp.).

Peptides in 0.1% formic acid/water were loaded from a cooled (10 °C) autosampler tray to a precolumn (Symmetry C18, 180 μm × 20 mm, 5 μm; Waters) and resolved on a BEH130 column (C18, 75 × 250 mm, 1.7 mm; Waters) in a gradient of 5–30% acetonitrile/water for 70 min at a flow rate of 0.3 μl/min. The ultra-performance LC system was directly connected to the ion source of the mass spectrometer. All MS runs were separated by blank runs to reduce the carry-over of peptides from previous samples. The mass spectrometer resolution was set to 50,000 for MS acquisitions, with an m/z measurement range of 300–2000 Th, and up to 10 fragmentation events were allowed for each parent ion. Data sets of parent and daughter ions were processed using MascotDistiller version 2.6.1 software (MatrixScience). The Mascot search engine (version 2.5.1) was used to survey data against the UniProtKB/Swiss-Prot database (Swissprot 2016_02; 552,259 sequences; 197,423,140 residues). The Mascot search parameters were set to the following: taxonomy (*Mus musculus*), variable modifications (cysteine carbamidomethylation or *N*-ethylmaleimide, methionine oxidation, peptide tolerance (5 ppm), fragment mass tolerance (5 ppm). Enzyme specificity was set to trypsin with one missed or nonspecific cleavage permitted. All obtained data were merged into one selected peptide list using MascotScan software (RRID:SCR_018201). The selected peptide list consists of sequences of peptides with Mascot scores exceeding the threshold value corresponding to <5% expectation value and false discovery rate < 1%. The lists of the peptide sequences that were identified in all of the LC-MS/MS runs from $Zdhhc7^{+/+}$ (control; $n = 3$) and $Zdhhc7^{-/-}$ (KO; $n = 3$) mice are presented in Table S2. Subsequently, probable contaminants (keratin and albumin) were removed from the analysis. For evaluation of the relative protein abundance in each sample, spectral count values determined using exponentially modified protein abundance index scores were used. Only proteins that met the acceptance criteria (false discovery rate < 1%, at least two unique peptides, Mascot score over 30, nonredundant proteins) were taken for further analysis.

Immunofluorescence analysis and imaging

Mouse kidneys were perfused with 4% paraformaldehyde, immersed in sucrose, and stored at −80 °C. Kidney cryosec-

tions (10-μm slices) were cut on a cryotome from Thermo Scientific (Microm HM560) and subjected to immunofluorescence analysis. The following primary antibodies were used: anti-barttin (#sc-49611), anti-AQP2 (aquaporin 2) (H40) (#sc-28629), and anti-V-ATPase B1/2 (F-6) (#sc-55544) from Santa Cruz Biotechnology and anti-CLC-K from Alomone Lab (#ACL-004). Alexa Fluor secondary antibodies were from Jackson Immunoresearch. Slices were mounted in anti-quenching medium (Fluoromount G, Southern Biotechnology Associates, Biozol, Eching, Germany). Imaging was performed by a confocal laser-scanning microscope Zeiss 710 (Carl Zeiss). Subcellular distribution of transiently expressed constructs in living MDCK II cells was analyzed by a confocal laser-scanning microscope, Zeiss 780 (Carl Zeiss), using a ×40 water immersion objective. The cells were imaged using online fingerprint mode enabling for the spectral unmixing.

Histology and imaging

CO_2-narcotized animals were sacrificed by intracardiac perfusion with 4% paraformaldehyde in PBS (pH 7.4). After preparation, the kidneys were fixed in 4% paraformaldehyde, dehydrated, and embedded in paraffin. Sections (2–4 μm thick) were deparaffinized in xylene and stained according to standard protocols. For detailed morphological investigations, hematoxylin and eosin stain, periodic acid–Schiff reaction, and a silver stain (Jones stain) were performed on serial sections. Morphologic evaluation (Axioskop 40, Zeiss microscope) was performed by a trained pathologist, and representative microphotographs were taken (AxioCam MRc, Zeiss).

Low-salt diet experiment and blood measurements

For *in vivo* experiments, 3-month-old male *Zdhhc7*$^{+/+}$ (WT) and *Zdhhc7*$^{-/-}$ (KO) mice (27) were subjected to standard diet (Na 2181.580 mg/kg; Cl 3628.760 mg/kg; K 6961.760 mg/kg) or to low-salt diet (Na 130.590 mg/kg; Cl 113.548 mg/kg; K 7088,293 mg/kg) for 12 days with water *ad libitum*. Both diets were purchased from Altromin (Germany). Volumes of remaining water in the drinking bottles were noted every day. For blood collection, mice were anesthetized by 4.5% isoflurane, and blood was collected from the retro-orbital sinus via a glass capillary coated with lithium EDTA and collected in a likewise coated vial to prevent coagulation. Blood measurements were prepared using blood gas analyzer ABL800FleX (Radiometer, Copenhagen, Denmark). After blood collection, animals were euthanized by cervical dislocation, and dissected kidneys were shock-frozen in liquid nitrogen and stored at −80 °C before the ABE analysis.

Statistical analysis

For statistical analyses, GraphPad Prism 7.0 was used. Data are represented as means ± S.D. or means + S.D. from at least three independent experiments. Significance was calculated by two-tailed unpaired Student's *t* test or one-way ANOVA (Dunnett's multiple-comparison test; for qPCR, Tukey's multiple-comparison test was used). *, $p < 0.05$; **, $p < 0.01$; ***, $p < 0.001$. Electrophysiological data analyses were performed using a software combination of Clampfit, SigmaPlot, and GraphPad Prism. Data are shown as mean values ± S.E.M. or mean values + S.D. Student's *t* test was performed to determine significant changes of mean current amplitudes.

Data availability

The mass spectrometry proteomics data have been deposited to the ProteomeXchange Consortium via the PRIDE partner repository with the data set identifier PXD017231. These data are publicly released. All data supporting the findings of this study are available within the article and its supporting information or are available from the corresponding author upon reasonable request.

Author contributions—N. G., D. W., A. Z., and V. E. software; N. G., D. W., D. G., D. A. G., F. E. M., A. W., S. T., A. Z., M. Z.-K., B. V. S., S. G., M. F., S. A.-S., N. K., C. H., W. Z., and V. E. validation; N. G., D. W., D. G., D. A. G., F. E. M., A. W., S. T., S. S., M. Z.-K., B. V. S., S. G., M. F., S. A.-S., N. K., C. H., W. Z., and V. E. investigation; N. G., D. G., A. W., A. Z., M. Z.-K., S. G., and C. H. visualization; N. G., D. W., D. G., D. A. G., F. E. M., A. W., A. Z., S. S., M. Z.-K., J. W., B. V. S., S. G., M. F., S. A.-S., N. K., C. H., W. Z., V. E., and E. P. methodology; N. G. and E. P. writing-original draft; S. T., J. W., M. F., W. Z., D. W., V. E., and E. P. writing-review and editing; J. W., M. F., W. Z., V. E., and E. P. supervision; J. W., W. Z., and E. P. funding acquisition; J. W., M. F., W. Z., and E. P. project administration; B. V. S. resources; E. P. conceptualization.

Acknowledgments—We thank Dr. Masaki Fukata for providing DHHC plasmids and Petra Killian and Stefanie Edler for technical assistance.

References

1. Watanabe, S., Fukumoto, S., Chang, H., Takeuchi, Y., Hasegawa, Y., Okazaki, R., Chikatsu, N., and Fujita, T. (2002) Association between activating mutations of calcium-sensing receptor and Bartter's syndrome. *Lancet* **360,** 692–694 CrossRef Medline
2. Birkenhäger, R., Otto, E., Schürmann, M. J., Vollmer, M., Ruf, E.-M., Maier-Lutz, I., Beekmann, F., Fekete, A., Omran, H., Feldmann, D., Milford, D. V., Jeck, N., Konrad, M., Landau, D., Knoers, N. V. A. M., Antignac, C., Sudbrak, R., Kispert, A., and Hildebrandt, F. (2001) Mutation of *BSND* causes Bartter syndrome with sensorineural deafness and kidney failure. *Nat. Genet.* **29,** 310–314 CrossRef Medline
3. Janssen, A. G. H., Scholl, U., Domeyer, C., Nothmann, D., Leinenweber, A., and Fahlke, C. (2009) Disease-causing dysfunctions of barttin in Bartter syndrome type IV. *J. Am. Soc. Nephrol.* **20,** 145–153 CrossRef Medline
4. Scholl, U., Hebeisen, S., Janssen, A. G. H., Müller-Newen, G., Alekov, A., and Fahlke, C. (2006) Barttin modulates trafficking and function of ClC-K channels. *Proc. Natl. Acad. Sci. U.S.A.* **103,** 11411–11416 CrossRef Medline
5. Waldegger, S., Jeck, N., Barth, P., Peters, M., Vitzthum, H., Wolf, K., Kurtz, A., Konrad, M., and Seyberth, H. W. (2002) Barttin increases surface expression and changes current properties of ClC-K channels. *Pflugers Arch.* **444,** 411–418 CrossRef Medline
6. Sands, J. M., and Layton, H. E. (2009) The physiology of urinary concentration: an update. *Semin. Nephrol.* **29,** 178–195 CrossRef Medline
7. Fahlke, C., and Fischer, M. (2010) Physiology and pathophysiology of ClC-K/barttin channels. *Front. Physiol.* **1,** 155 CrossRef Medline
8. Steinke, K. V., Gorinski, N., Wojciechowski, D., Todorov, V., Guseva, D., Ponimaskin, E., Fahlke, C., and Fischer, M. (2015) Human CLC-K channels require palmitoylation of their accessory subunit Barttin to be functional. *J. Biol. Chem.* **290,** 17390–17400 CrossRef Medline
9. Adachi, N., Hess, D. T., McLaughlin, P., and Stamler, J. S. (2016) *S*-Palmitoylation of a novel site in the β_2-adrenergic receptor associated with a novel intracellular itinerary. *J. Biol. Chem.* **291,** 20232–20246 CrossRef Medline

10. Chen, S., Han, C., Miao, X., Li, X., Yin, C., Zou, J., Liu, M., Li, S., Stawski, L., Zhu, B., Shi, Q., Xu, Z.-X., Li, C., Goding, C. R., Zhou, J., and Cui, R. (2019) Targeting MC1R depalmitoylation to prevent melanomagenesis in redheads. *Nat. Commun.* **10,** 877 CrossRef Medline
11. Mitchell, D. A., Vasudevan, A., Linder, M. E., and Deschenes, R. J. (2006) Thematic review series: lipid posttranslational modifications. Protein palmitoylation by a family of DHHC protein *S*-acyltransferases. *J. Lipid Res.* **47,** 1118–1127 CrossRef Medline
12. Ohno, Y., Kihara, A., Sano, T., and Igarashi, Y. (2006) Intracellular localization and tissue-specific distribution of human and yeast DHHC cysteine-rich domain-containing proteins. *Biochim. Biophys. Acta* **1761,** 474–483 CrossRef Medline
13. Fukata, M., Fukata, Y., Adesnik, H., Nicoll, R. A., and Bredt, D. S. (2004) Identification of PSD-95 palmitoylating enzymes. *Neuron* **44,** 987–996 CrossRef Medline
14. Du, K., Murakami, S., Sun, Y., Kilpatrick, C. L., and Luscher, B. (2017) DHHC7 palmitoylates glucose transporter 4 (Glut4) and regulates Glut4 membrane translocation. *J. Biol. Chem.* **292,** 2979–2991 CrossRef Medline
15. Fang, C., Deng, L., Keller, C. A., Fukata, M., Fukata, Y., Chen, G., and Lüscher, B. (2006) GODZ-mediated palmitoylation of GABAA receptors is required for normal assembly and function of GABAergic inhibitory synapses. *J. Neurosci.* **26,** 12758–12768 CrossRef Medline
16. Tsutsumi, R., Fukata, Y., Noritake, J., Iwanaga, T., Perez, F., and Fukata, M. (2009) Identification of G protein α subunit-palmitoylating enzyme. *Mol. Cell. Biol.* **29,** 435–447 CrossRef Medline
17. Chen, S., Zhu, B., Yin, C., Liu, W., Han, C., Chen, B., Liu, T., Li, X., Chen, X., Li, C., Hu, L., Zhou, J., Xu, Z.-X., Gao, X., Wu, X., Goding, C. R., and Cui, R. (2017) Palmitoylation-dependent activation of MC1R prevents melanomagenesis. *Nature* **549,** 399–403 CrossRef Medline
18. Yanai, A., Huang, K., Kang, R., Singaraja, R. R., Arstikaitis, P., Gan, L., Orban, P. C., Mullard, A., Cowan, C. M., Raymond, L. A., Drisdel, R. C., Green, W. N., Ravikumar, B., Rubinsztein, D. C., El-Husseini, A., and Hayden, M. R. (2006) Palmitoylation of huntingtin by HIP14 is essential for its trafficking and function. *Nat. Neurosci.* **9,** 824–831 CrossRef Medline
19. Raymond, F. L., Tarpey, P. S., Edkins, S., Tofts, C., O'Meara, S., Teague, J., Butler, A., Stevens, C., Barthorpe, S., Buck, G., Cole, J., Dicks, E., Gray, K., Halliday, K., Hills, K., *et al.* (2007) Mutations in ZDHHC9, which encodes a palmitoyltransferase of NRAS and HRAS, cause X-linked mental retardation associated with a marfanoid habitus. *Am. J. Hum. Genet.* **80,** 982–987 CrossRef Medline
20. Yamamoto, Y., Chochi, Y., Matsuyama, H., Eguchi, S., Kawauchi, S., Furuya, T., Oga, A., Kang, J. J., Naito, K., and Sasaki, K. (2007) Gain of 5p15.33 is associated with progression of bladder cancer. *Oncology* **72,** 132–138 CrossRef
21. Saleem, A. N., Chen, Y.-H., Baek, H. J., Hsiao, Y.-W., Huang, H.-W., Kao, H.-J., Liu, K.-M., Shen, L.-F., Song, I., Tu, C.-P. D., Wu, J.-Y., Kikuchi, T., Justice, M. J., Yen, J. J. Y., and Chen, Y.-T. (2010) Mice with alopecia, osteoporosis, and systemic amyloidosis due to mutation in Zdhhc13, a gene coding for palmitoyl acyltransferase. *PLoS Genet.* **6,** e1000985 CrossRef Medline
22. Roy, K., Jerman, S., Jozsef, L., McNamara, T., Onyekaba, G., Sun, Z., and Marin, E. P. (2017) Palmitoylation of the ciliary GTPase ARL13b is necessary for its stability and its role in cilia formation. *J. Biol. Chem.* **292,** 17703–17717 CrossRef Medline
23. Mukherjee, A., Mueller, G. M., Kinlough, C. L., Sheng, N., Wang, Z., Mustafa, S. A., Kashlan, O. B., Kleyman, T. R., and Hughey, R. P. (2014) Cysteine palmitoylation of the γ subunit has a dominant role in modulating activity of the epithelial sodium channel. *J. Biol. Chem.* **289,** 14351–14359 CrossRef Medline
24. McHaffie, G. S., Graham, C., Kohl, B., Strunck-Warnecke, U., and Werner, A. (2007) The role of an intracellular cysteine stretch in the sorting of the type II Na/phosphate cotransporter. *Biochim. Biophys. Acta* **1768,** 2099–2106 CrossRef Medline
25. Fukata, Y., and Fukata, M. (2010) Protein palmitoylation in neuronal development and synaptic plasticity. *Nat. Rev. Neurosci.* **11,** 161–175 CrossRef Medline
26. Ernst, A. M., Syed, S. A., Zaki, O., Bottanelli, F., Zheng, H., Hacke, M., Xi, Z., Rivera-Molina, F., Graham, M., Rebane, A. A., Björkholm, P., Baddeley, D., Toomre, D., Pincet, F., and Rothman, J. E. (2018) *S*-Palmitoylation sorts membrane cargo for anterograde transport in the Golgi. *Dev. Cell.* **47,** 479–493.e7 CrossRef Medline
27. Hohoff, C., Zhang, M., Ambrée, O., Kravchenko, M., Buschert, J., Kerkenberg, N., Gorinski, N., Abdel Galil, D., Schettler, C., Vom Werth, K. L., Wewer, M. F.-J., Schneider, I., Grotegerd, D., Wachsmuth, L., Faber, C., *et al.* (2019) Deficiency of the palmitoyl acyltransferase ZDHHC7 impacts brain and behavior of mice in a sex-specific manner. *Brain Struct. Funct.* **224,** 2213–2230 CrossRef Medline
28. Akahoshi, N., Kamata, S., Kubota, M., Hishiki, T., Nagahata, Y., Matsuura, T., Yamazaki, C., Yoshida, Y., Yamada, H., Ishizaki, Y., Suematsu, M., Kasahara, T., and Ishii, I. (2014) Neutral aminoaciduria in cystathionine β-synthase-deficient mice, an animal model of homocystinuria. *Am. J. Physiol. Renal Physiol.* **306,** F1462–F1476 CrossRef Medline
29. Fujita, H., Hamazaki, Y., Noda, Y., Oshima, M., and Minato, N. (2012) Claudin-4 deficiency results in urothelial hyperplasia and lethal hydronephrosis. *PLoS ONE* **7,** e52272 CrossRef Medline
30. Tagawa, H., Kizuka, Y., Ikeda, T., Itoh, S., Kawasaki, N., Kurihara, H., Onozato, M. L., Tojo, A., Sakai, T., Kawasaki, T., and Oka, S. (2005) A non-sulfated form of the HNK-1 carbohydrate is expressed in mouse kidney. *J. Biol. Chem.* **280,** 23876–23883 CrossRef Medline
31. Uchida, S., Sasaki, S., Nitta, K., Uchida, K., Horita, S., Nihei, H., and Marumo, F. (1995) Localization and functional characterization of rat kidney-specific chloride channel, ClC-K1. *J. Clin. Invest.* **95,** 104–113 CrossRef Medline
32. Estévez, R., Boettger, T., Stein, V., Birkenhäger, R., Otto, E., Hildebrandt, F., and Jentsch, T. J. (2001) Barttin is a Cl^- channel β-subunit crucial for renal Cl^- reabsorption and inner ear K^+ secretion. *Nature* **414,** 558–561 CrossRef Medline
33. Zareba-Koziol, M., Bartkowiak-Kaczmarek, A., Figiel, I., Krzystyniak, A., Wojtowicz, T., Bijata, M., and Wlodarczyk, J. (2019) Stress-induced changes in the *S*-palmitoylation and *S*-nitrosylation of synaptic proteins. *Mol. Cell. Proteomics* **18,** 1916–1938 CrossRef Medline
34. Nomura, N., Tajima, M., Sugawara, N., Morimoto, T., Kondo, Y., Ohno, M., Uchida, K., Mutig, K., Bachmann, S., Soleimani, M., Ohta, E., Ohta, A., Sohara, E., Okado, T., Rai, T., *et al.* (2011) Generation and analyses of R8L barttin knockin mouse. *Am. J. Physiol. Renal Physiol.* **301,** F297–F307 CrossRef Medline
35. Kilpatrick, C. L., Murakami, S., Feng, M., Wu, X., Lal, R., Chen, G., Du, K., and Luscher, B. (2016) Dissociation of Golgi-associated DHHC-type zinc finger protein (GODZ)- and Sertoli cell gene with a zinc finger domain-β (SERZ-β)-mediated palmitoylation by loss of function analyses in knockout mice. *J. Biol. Chem.* **291,** 27371–27386 CrossRef Medline
36. Pinelli, L., Nissant, A., Edwards, A., Lourdel, S., Teulon, J., and Paulais, M. (2016) Dual regulation of the native ClC-K2 chloride channel in the distal nephron by voltage and pH. *J. Gen. Physiol.* **148,** 213–226 CrossRef Medline
37. Tajima, M., Hayama, A., Rai, T., Sasaki, S., and Uchida, S. (2007) Barttin binds to the outer lateral surface of the ClC-K2 chloride channel. *Biochem. Biophys. Res. Commun.* **362,** 858–864 CrossRef Medline
38. Gubitosi-Klug, R. A., Mancuso, D. J., and Gross, R. W. (2005) The human Kv1.1 channel is palmitoylated, modulating voltage sensing: identification of a palmitoylation consensus sequence. *Proc. Natl. Acad. Sci. U.S.A.* **102,** 5964–5968 CrossRef Medline
39. Shipston, M. J. (2014) Ion channel regulation by protein *S*-acylation. *J. Gen. Physiol.* **143,** 659–678 CrossRef Medline
40. García-Nieto, V., Flores, C., Luis-Yanes, M. I., Gallego, E., Villar, J., and Claverie-Martín, F. (2006) Mutation G47R in the BSND gene causes Bartter syndrome with deafness in two Spanish families. *Pediatr. Nephrol.* **21,** 643–648 CrossRef Medline
41. Rana, M. S., Kumar, P., Lee, C.-J., Verardi, R., Rajashankar, K. R., and Banerjee, A. (2018) Fatty acyl recognition and transfer by an integral membrane *S*-acyltransferase. *Science* **359,** eaao6326 CrossRef Medline
42. Degasperi, A., Birtwistle, M. R., Volinsky, N., Rauch, J., Kolch, W., and Kholodenko, B. N. (2014) Evaluating strategies to normalise biological replicates of Western blot data. *PLoS ONE* **9,** e87293 CrossRef Medline
43. Yokoi, N., Fukata, Y., Sekiya, A., Murakami, T., Kobayashi, K., and Fukata, M. (2016) Identification of PSD-95 depalmitoylating enzymes. *J. Neurosci.* **36,** 6431–6444 CrossRef Medline